Pulsed Field Gradient Nuclear Magnetic Resonance Study of Time-Dependent Diffusion Behavior and Exchange of Lipids in Planar-Supported Lipid Bilayers

Monica Sanders, Robert Mueller, Amrish Menjoge, and Sergey Vasenkov*

Department of Chemical Engineering, University of Florida, Gainesville, Florida 32611

Received: June 17, 2009; Revised Manuscript Received: September 4, 2009

This work reports the direct experimental observation of lipid exchange between liquid-ordered domains and their liquid-disordered surroundings in 3-component planar-supported multibilayers (1,2-dioleoyl-*sn*-glycerol-3-phosphocholine/1,2-dipalmitoyl-*sn*-glycero-3-phosphocholine/cholesterol). The measurements of lipid lateral diffusion and exchange were carried out using proton pulsed field gradient (PFG) NMR spectroscopy with high field strength (17.6 T) and high gradient amplitudes (up to 30 T/m). Application of large gradients affords the use of sufficiently small diffusion times under the condition that the width of the gradient pulses is much smaller than the diffusion time. As a result, PFG NMR studies of time-dependent diffusion behavior in lipid bilayers become possible over submicrometer length scales of displacements, which are comparable with the domain size. Comparison of the PFG NMR diffusion data and the corresponding results of dynamic Monte Carlo simulations allowed for the estimation of domain boundary permeability and domain size at temperatures near the transition temperature for the studied bilayers.

Introduction

Lipid membranes consisting of ternary mixtures of saturated and unsaturated phospholipids, sphingolipids, and cholesterol are considered suitable models for studying the lateral organization of biological membranes.[1] Compositional inhomogeneities in eukaryotic cell membranes have attracted the interest of the research community since at least the early 1970s, which marks the introduction of the "fluid mosaic model".[2] The lipid raft hypothesis further stimulated interest by postulating the existence of small functional domains, lipid rafts, which are characterized by an enhanced concentration of cholesterol as well as other lipids and proteins.[3] Lipid rafts are believed to play roles in cellular functions such as signal transduction[4] as well as cancer cell proliferation[5] and viral particle penetration into the cell.[6] In vivo studies are complicated by the sheer complexity of the cell membrane. Studies using model membranes can provide fundamental understanding of cell membrane properties by observing behavior in less complex multicomponent bilayers. The liquid-ordered (l_o) phase which can easily be observed in cholesterol- and sphingolipid-rich model membranes has been closely linked to lipid rafts present in the eukaryotic cell membrane.[1,7,8]

In order to most accurately study the organization and dynamics of domains either in vivo or in model membranes, an experimental technique must be utilized which has the appropriate spatial and temporal resolution and does not perturb the membrane organization. Many studies are carried out by microscopy techniques such as fluorescence resonance energy transfer (FRET), fluorescence recovery after photobleaching (FRAP), and fluorescence correlation spectroscopy (FCS).[9−15] These methods have proven to be useful in detecting domains and studying the dynamics inside domains; however, they are limited by the optical diffraction limit and the observation that fluorescent labels can affect the physical properties of small biomolecules, such as lipids, in the membranes.[16] Methods such as single particle (molecule) tracking as well as improved FCS methods which allow the resolution to go beyond the optical diffraction limit provide better spatial resolution[17−22] but are still limited by the requirement of labels. Nuclear magnetic resonance (NMR) techniques such as magic angle spinning (MAS) NMR and pulsed field gradient (PFG) NMR as well as the combination of these two techniques (MAS PFG NMR) offer a way to study membrane domains without requiring the attachment of labels to membrane molecules.[23−29] Recently, the PFG NMR technique using high magnetic field gradient amplitudes (up to 30 T/m) was employed by the authors of this paper to study lipid dynamics in model membranes over length scales relevant for studies of lipid rafts.[30,31]

Liquid-ordered domains in model membranes have been seen to be quite large (in most cases much larger than 1 μm) in comparison to those in biomembranes which are expected to be on the order of or smaller than 300 nm[32,33] and quite unstable.[34] Recent progress by a number of techniques including FRET,[10,11] AFM,[19−21] and solid state NMR[24,35,36] gives evidence for domain sizes in the range of 100 nm in model membranes. Such domains have been observed to be stable even at physiological temperatures when the same membrane would appear homogeneous by other methods.[37] The size of domains have been shown to be both a function of temperature and composition.[35,38] As the temperature of the raft-containing bilayer is increased to approach the miscibility transition temperature, T_m, large micrometer-sized domains are expected to be replaced by smaller domains. Critical fluctuations are expected when the system is very near T_m. These fluctuations are on the length scale of <50 nm.[38] Such fluctuations represent the formation and collapse of complexes consisting for the most part of a small number of cholesterol molecules and saturated lipids.[39] It has been suggested that critical fluctuations can be viewed as the onset of raft formation,[40] which involves cholesterol's affinity for and dynamic relationship with saturated lipids.[41−43] Studies of nanodomains are still in the early stages of a journey to understanding the formation and function of lipid rafts in cell membranes. It is, however, quite clear that exchange of lipids between rafts and their surroundings plays a

* E-mail: svasenkov@che.ufl.edu.

10.1021/jp9057093 CCC: $40.75
Published on Web 10/01/2009

key role in raft formation. Here, we report a direct observation of such exchange using PFG NMR at high field (17.6 T) and high magnetic field gradient strengths (up to 30 T/m). The application of high gradients opens up the possibility of studies of diffusion for short diffusion times under the conditions of the narrow-pulse approximation,[44,45] which allows for distortion-free monitoring of time-dependent and displacement-dependent diffusivities. Such diffusivities are expected in lipid bilayers when molecular displacements are comparable with the raft sizes. It is feasible to satisfy this condition with our experimental setup which is capable of monitoring diffusion over length scales as small as 100 nm.[30,31] The PFG NMR diffusion measurements have been performed with the commonly used ternary lipid bilayers exhibiting formation of raftlike domains.[24,35,46,47] Diffusion data was used to obtain information about domain sizes and the permeability of the domain boundaries.

Experimental Section

Oriented Multibilayer Stacks. PFG NMR studies were performed with multibilayer stacks supported on thin glass plates. The bilayer stacks were prepared from ternary lipid mixtures of 1,2-dioleoyl-*sn*-glycero-3-phosphocholine (DOPC, >99%), 1,2-dipalmitoyl-*sn*-glycero-3-phosphocholine (DPPC, >99%), and cholesterol (CHOL, >99%). DOPC and DPPC were purchased from Avanti Polar Lipid, Inc. (Alabaster, AL), while CHOL was supplied by Sigma-Aldrich (St. Louis, MO). Sample preparation methods for bilayers reconstituted on glass planar supports have been discussed in detail in our previous work.[30] Briefly, each lipid is dissolved in a solvent solution, and the three individual lipid stock solutions are combined such that the mixture is 35% DOPC, 35% DPPC, and 30% CHOL on a molar basis. A sublimable solid, i.e., naphthalene obtained from Cambridge Isotope Laboratories (Andover, MA), was then introduced into the lipid mixture in a naphthalene:lipid molar ratio of 1:1. The resulting solution was deposited onto clean glass plates (5×5 mm^2 with a plate thickness of $\sim$0.1 mm) obtained from Marienfeldt/Menzel (Lauda-Königshofen/Braunschweig, Germany), and the solvent was evaporated off overnight under high vacuum at $\sim$313 K. After solvent evaporation, the plates were left unstacked and hydrated from the gas phase in the presence of liquid ^2H_2O saturated with K_2SO_4 (97% relative humidity) obtained from Spectra Stable Isotopes (Columbia, MD) and Sigma-Aldrich (St. Louis, MO), respectively for 2 days inside of a hydration chamber. After the initial hydration step, pure liquid ^2H_2O was directly added to the lipid bilayers using a syringe. The 30−35 plates were stacked and then held at 277 K for an additional 2 days. Once the stack is set up inside the NMR tube (see next section for details), pure ^2H_2O is added to maintain the sample at maximum (i.e., 100%) hydration. The previous studies of the authors of this paper and their colleagues have demonstrated that such procedure results in the formation of oriented multibilayer stacks.[30,31]

NMR Measurements. ^{1}H PFG NMR measurements of lipids in lipid membranes are complicated by rather short transversal (T_2) NMR relaxation times and the related large line width of NMR spectra. Short T_2 times and the related line broadening are mainly caused by strong proton dipole−dipole interactions in lipids that are not completely averaged out by molecular motion. The scaling factor in the Hamiltonian term describing these dipole−dipole interactions is $(3 \cos^2 \theta - 1)$, where θ is the angle between the dipole moment of the lipids and the direction of the applied magnetic field B_0. In order to minimize the effects of dipole−dipole interactions on T_2 times and hence line width, the stack of glass plates with bilayers was oriented in the NMR spectrometer in such a way that θ is very close to the so-called "magic" angle (54.7°) corresponding to the scaling factor equal to zero. To orient the bilayer stacks at the magic angle, a special insert was developed and tested for use with commercially available high-gradient diffusion probes.[30,31] The stacks were placed in the insert and inside a 10 mm NMR tube along with a few drops of excess ^2H_2O added below the sample to ensure that the relative humidity in the gas phase surrounding the bilayers is 100%. The measurements of self-diffusion in model lipid bilayers were carried out on a wide-bore Bruker PFG NMR spectrometer operating at a ^{1}H resonance frequency of 750 MHz located at the Advanced Magnetic Resonance Imaging and Spectroscopy (AMRIS) facility of University of Florida in Gainesville, FL. A Diff60 probe with a GREAT60 amplifier was used to generate high gradients for diffusion measurements. To measure diffusivity, the PFG NMR signal $A(g)$ obtained using a standard stimulated echo sequence was measured as a function of the magnitude of applied field gradient (g). The amplitudes of line corresponding to proton signal from the choline-$(CH_3)_3$ headgroup in the NMR spectra were used as a measured signal to obtain PFG NMR attenuation curves. T_2 NMR relaxation times for this group were larger than the alternative (i.e., the methylene CH_2 groups in the hydrocarbon chains) as will be discussed in the next section. The diffusivities D were obtained from either a one-exponential or two-exponential fit of the PFG NMR attenuation curves using

$$\Psi \equiv \frac{A(g)}{A(g=0)} = \sum_{i=1}^{n=1\text{or}2} p_i \exp(-q^2 t_{\text{eff}} D_i^{\text{m}}) \qquad (1)$$

where $q = \gamma\delta g$ for the stimulated echo sequence. γ is the gyromagnetic ratio, δ denotes the duration of the pulsed field gradient, t_{eff} is the effective diffusion time,[48] and p_i is the fraction of molecules diffusing with a diffusivity D_i^{m}. Values of δ and t_{eff} were kept constant for measurement of each attenuation curve. NMR relaxation can influence the determination of p_i as will be discussed in detail later in this work. Acquisition of each proton spectrum using the PFG NMR sequences most often required only 16 scans. The resulting ratios of signal-to-noise at small gradient strengths were around 200. Effective diffusion times and temperatures were varied in the range of 8.24−239.24 ms and 291−310 K, respectively. The diffusion probe used is suitable for PFG NMR measurements with gradient amplitudes up to 30 T/m, but a maximum of 28 T/m was needed for most of our experiments. Typically, the signal at 16 or 20 gradient strengths was recorded to obtain each PFG NMR attenuation curve. The diffusivities determined by fitting the attenuation curves using eq 1 correspond to the diffusion along the direction that coincides with the direction of the gradients and that of B_0. This direction was different from that of lateral diffusion. Diffusivities were then multiplied by a factor of 1.5 to obtain the correct values for lateral diffusion.[49]

Dynamic Monte Carlo Simulations. Complementary dynamic Monte Carlo (MC) simulations of molecular diffusion on a square lattice were performed to extract information on the permeability of the domain boundaries and domain sizes from the measured PFG NMR data. Such simulations as well as the procedure of fitting PFG NMR results by the corresponding results of simulations to estimate permeabilities and domain sizes were recently reported in several papers.[50−53] Briefly, in complete analogy with the lattice described in ref 45, the two-dimensional simulation lattice used in this work consists of four square domains representing domains of liquid-ordered phase

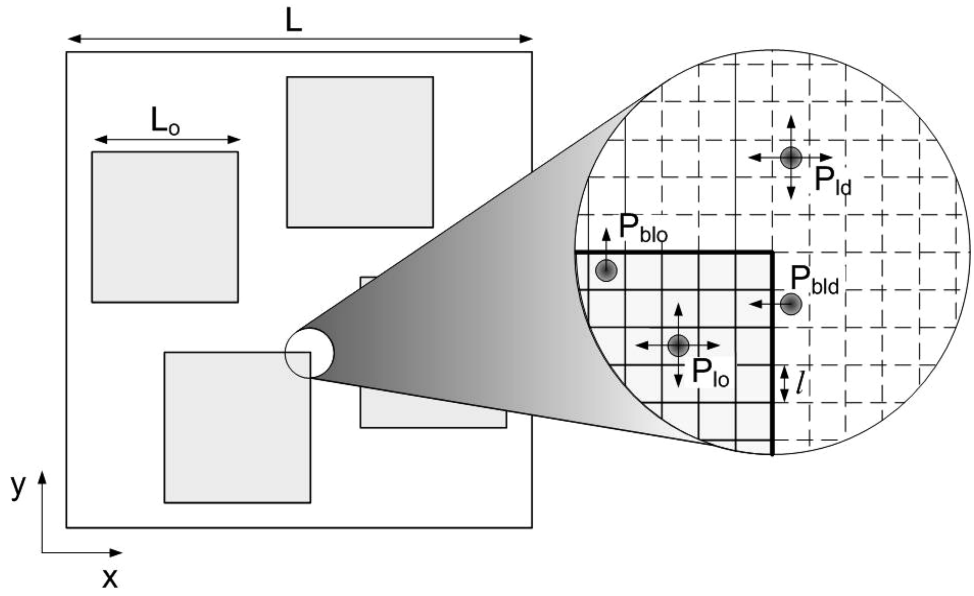

Figure 1. Two-dimensional simulation model for lipid bilayer. The periodic structure is organized by repetition of the simulation lattice of length L. The square domains of length L_o represent the liquid-ordered phase (l_o), and the surrounding interdomain lattice represents the liquid-disordered phase (l_d). The inset shows various jump probabilities and the elementary diffusion step used in the simulation model.

(l_o) that are surrounded by the interdomain lattice representing the liquid-disordered phase (l_d) (Figure 1). The size of the simulation lattice shown in Figure 1 was $L \times L$ ($L = 262l$, where l is the length of the elementary diffusion step) and the size of the l_o domains was $L_o \times L_o$ ($L_o = 92l$). Lipid diffusion was simulated by random walk on this lattice. Periodic boundary conditions were applied at the lattice boundaries. The probability of an elementary diffusion step inside the l_o domains in the x or y direction is denoted as p_{l_o} and that through the domain boundary leading into the l_d phase is denoted as p_{bl_o} ($1 \leq p_{l_o}/p_{bl_o} \leq 1000$). The corresponding probability of an elementary diffusion step inside the l_d interdomain spaces in the x or y direction is denoted as p_{l_d} and that through the domain boundary leading into the l_o phase is denoted as p_{bl_d}. The experimentally observed difference between the diffusivities in the l_o and l_d phases was taken into account by choosing $p_{l_d}/p_{l_o} = 2$ resulting in $p_{bl_d}/p_{bl_o} = 2$. The starting points of 10 000 random walkers were randomly selected on the lattice. The N-step walks ($N \leq 10\,000$) were then generated for each random walker. The final simulations results reported in this paper were the averages over three lattices with different configurations of the starting points. The quantities recorded in the simulation were the relative number of labeled random walkers, i.e., those that were inside an l_o domain at the time $t = 0$ and were still inside the same domain at a later time t, ($N(t)/N_0$, where $N_0 = N(t = 0)$), as well as normalized effective diffusivity of these random walkers, $D_0(t)/D_{0,t\to 0}$, where $D_{0,t\to 0}$ is the diffusivity inside the l_o domain at sufficiently small time when the domain boundaries do not influence diffusion behavior. The diffusion time is defined as $t = N\tau$, where τ is the duration of the elementary diffusion step. The effective diffusivity $D_0(t)$ is calculated from the Einstein equation

$$\langle r^2(t)\rangle = 4Dt \tag{2}$$

where $\langle r^2(t)\rangle$ is the mean square displacement of a random walker at time t.

As a first approximation, since the data is collected for molecules that start their trajectories inside of a domain and are still located in that same domain at the specified diffusion time, the size of the domain surroundings is not very relevant to the data recorded in the simulations. As a result, similar simulations reported previously in refs 46−48 were performed with a single domain (i.e., zeolite crystal). Periodic boundary conditions were applied at the domain boundaries. Hence, the domain surroundings were not a part of the simulation lattice in that case. Taking into account that the properties of the domain surroundings are only of a minor importance for the recorded data, the simulations reported in this work were performed with the simulation lattice where the ratio between the total area of l_o domains and their surroundings only approximately corresponded to the ratio between the fractions of lipids in the l_d and l_o phases as observed by PFG NMR. In all cases, the ratio between the total area of l_o domains and their surroundings in the simulation lattice was equal to ~1. In contrast to the square shape of the domains used in the simulations, the true shape of domains in the bilayer is most likely circular. However, it has been shown that the shape of the domains has only a minor influence on the dynamic properties recorded in the simulations if the domains have the same ratio of the surface area to perimeter.[53] In order for comparison between domains in the simulation lattice and the lipid bilayers, an effective domain radius is determined using the respective surface area-to-perimeter ratios. On the basis of the formalism discussed in ref 45, the probability p_{bl_o} can be used for calculation of the permeability of the domain boundaries for molecules (α) as

$$\alpha = p_{bl_o}\frac{D_{0,t\to 0}}{l} \tag{3}$$

Varying p_{bl_o} is thus equivalent to varying α in our simulations.

Results

Figure 2 shows examples of ^{1}H NMR spectra of the oriented multibilayer stacks measured by the PFG NMR stimulated echo (STE) sequence under the measurement conditions used for diffusion studies. Both Figure 2A and B show spectra from

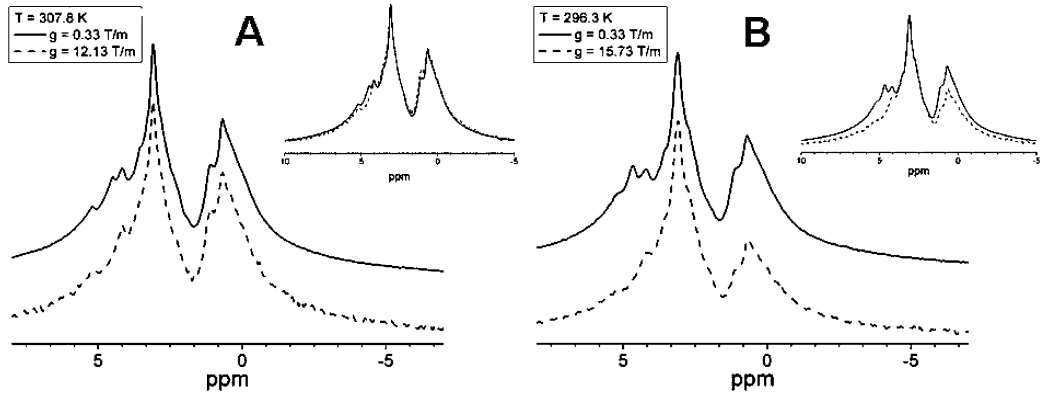

Figure 2. ^{1}H NMR spectra of multibilayer stacks measured by the stimulated echo sequence for different values of gradient amplitude (g) at $T =$ 307.8 K (A) and $T = 296.3$ K (B).

measurements at an initial gradient strength (solid) and an intermediate gradient strength (dashed). Each spectrum shows partially overlapping lines of the CH_2 groups of the hydrocarbon chains and of the CH_3 groups of lipid headgroups at around 1 and 3 ppm, respectively. This signal originates from the phospholipids. No signal from CHOL can be observed due to the short T_2 NMR relaxation times of this rigid molecule.[28] A line at around 4.7 ppm is assigned to a small amount of protonated water present in the sample. The smallest gradient strength (i.e., 0.33 T/m) was chosen in such a way that it was sufficiently small to ensure that there is no attenuation of the lipid signal, and at the same time, sufficiently high for suppression of any significant contribution of H_2O to the measured signal. The diffusivity of water in the lateral direction is around 2 orders of magnitude larger than that of lipids. Therefore, the water signal disappears at relatively small gradients under our experimental conditions. Figure 2A shows spectra obtained at $T = 307.8$ K, a temperature well above the miscibility transition temperature, T_m, for this sample, at gradient amplitudes of 0.33 and 12.13 T/m. Above the T_m, the bilayer is expected to be one homogeneous phase with a single lipid diffusivity. The inset in Figure 2A presents the two spectra superimposed where the spectrum obtained using the intermediate gradient strength is scaled such that the intensities of the CH_3 signals are equivalent. The coincidence in signal shape of the two spectra is nearly exact except for a small difference corresponding to the loss of water line. The change is minor and does not significantly affect the measurement of lipid self-diffusion.

Figure 2B shows spectra obtained at $T = 296.3$ K using gradient amplitudes of 0.33 and 15.73 T/m. The intermediate gradient strengths at each temperature correspond to approximately the same attenuation of signal. At lower temperatures, the diffusivities of lipids are smaller requiring larger gradient amplitudes to reach the same level of attenuation as that at a higher temperature. In the inset of Figure 2B, the two spectra are shown with the spectrum obtained using the intermediate gradient strength scaled such that the intensities of the CH_3 signals are equivalent. Unlike Figure 2A, the spectra show that the shapes of the NMR spectra depend on the applied gradient strength. The line corresponding to the CH_2 groups appears to attenuate at a larger rate than the line for the CH_3 group. This occurs because each spectrum obtained at this temperature is a superposition of signals coming from two components, a slow and a fast diffusion component[28] corresponding to diffusion inside liquid-ordered (l_o) and liquid-disordered (l_d) phases, respectively.[24,25] The l_o domains are enriched in DPPC and characterized by a tighter packing and lower diffusivity of lipids in comparison with the DOPC-enriched l_d phase. The NMR lines of CH_2 and CH_3 groups shown in Figure 2B have different contributions from both phases. The change in the shapes of the spectra that is seen in Figure 2B is a consequence of a larger decrease of the contribution from the phase with the highest diffusivity, i.e., the l_d phase, with increasing gradient strength. The spectra in Figure 2 show that in all cases the amplitude of the choline CH_3 line is larger than the amplitude of the CH_2 line despite the fact that fewer protons contribute to the former line than to the latter. This results from the influence of T_2 NMR relaxation.[28] Under the measurement conditions of the PFG NMR stimulated echo sequence, signal amplitude is reduced due to T_2 NMR relaxation by a factor of $\exp(-2\tau/T_2)$. As already mentioned above, in lipid bilayers the rate of T_2 NMR relaxation is enhanced by proton dipole−dipole interactions. Protons in the hydrocarbon chains of lipids are expected to have shorter T_2 NMR relaxation times in the l_o phase than in the l_d phase due to increased packing order in the former phase.[25] In comparison to protons in the hydrocarbon chain, protons in the head groups of lipids residing in both l_o and l_d phases have a higher flexibility with respect to reorientations. Hence, the T_2 times of these protons are less sensitive to dipole−dipole interactions resulting in larger T_2 values. Therefore the choline CH_3 line is used for obtaining diffusion data at all temperatures. For selected experiments, the data was treated using the amplitudes of the CH_2 line in the attenuation plots in order to verify that diffusion coefficients obtained from fits with eq 1 would agree with the data obtained using the CH_3 line. The only difference between the treatment of the two lines is the phase fractions obtained since the measured signal of the l_o phase is more significantly reduced by T_2. While signal amplitude is reduced for both lines, the CH_3 line is a better representative of the signal unperturbed by the T_2 NMR relaxation process.

Figure 3 shows examples of ^{1}H PFG NMR attenuation curves measured by the PFG NMR stimulated echo sequence for different effective diffusion times at five different temperatures. Fitting the attenuation curves in Figure 3A by eq 1 has shown that for $T = 307.8$ K it is sufficient to use the one-exponential curve (eq 1 with $n = 1$) in order to fit the experimental data satisfactorily. Single-exponential behavior corresponds to a single diffusivity for all lipids contributing to the measured signal. In the presentation of Figure 3, the curves obtained for different diffusion times are expected to coincide if the diffusivity of the probed lipids remains the same with increasing or decreasing diffusion time and the corresponding values of the mean square displacement. The data in this Figure 3A indicate that there is no dependence of the attenuation curves

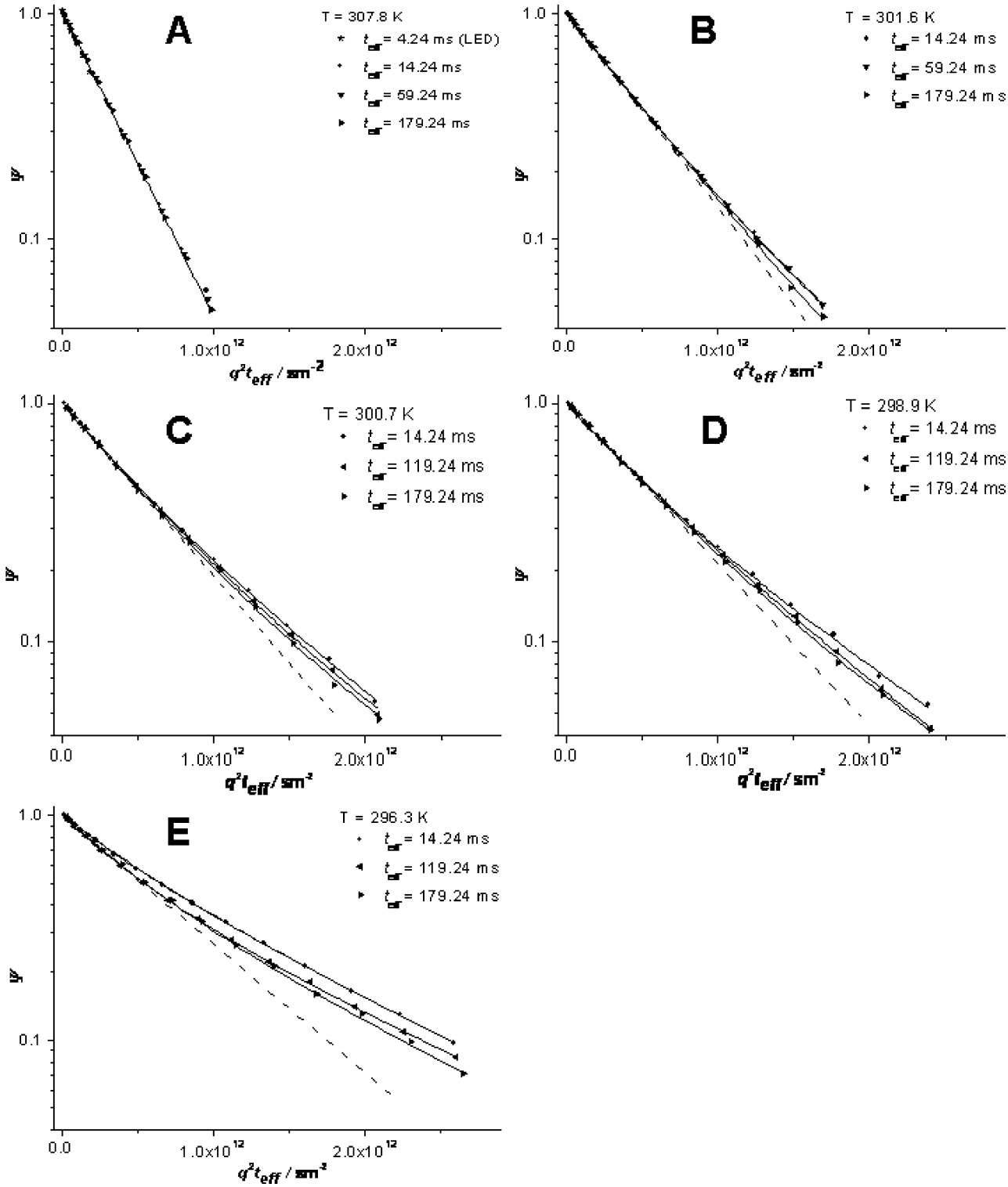

Figure 3. Examples of diffusion attenuation curves obtained by the PFG NMR stimulated echo sequence at $T = 307.8$ K (A), $T = 301.3$ K (B), $T = 300.7$ K (C), $T = 298.8$ K (D), and $T = 296.3$ K (E). All attenuation curves are obtained by measuring the intensity of the choline lines in the NMR spectra. In part A, the solid line is a single-exponential fit of all data in the figure. In parts B−E, solid lines are individual two-exponential fits of each curve using eq 1 with $n = 2$. The dash lines show monoexponential curves corresponding to the initial decay of the measured attenuation curves.

and of the corresponding diffusion behavior on diffusion time at 307.8 K. Hence, it can be concluded that all probed lipids diffuse with the same diffusivity, which is independent of diffusion time in the measured range.

Figure 3A displays one curve obtained by a sequence known as the PFG NMR stimulated echo longitudinal-encode-decode sequence (STE LED) measured with $t_{eff} = 4.24$ ms. In comparison to the traditional PFG NMR STE sequence, this sequence has an additional delay before the data acquisition to allow for a decay of eddy currents.[54] It is possible not only to compare results obtained using the STE and PFG NMR STE LED sequences to check for the influence of eddy currents but also to obtain results using much smaller t_{eff} (as low as 4.24 ms). In measurements with the former sequence, all essential

parameters such as the total duration of the gradient pulses, effective diffusion time, and temperature were kept to be the same or similar as in the measurements with the later sequence. As expected, no significant changes in the initial slope of attenuation curves (not shown) or the related effective diffusivity were observed when using the PFG NMR STE LED sequence.

Figure 3E is a collection of attenuation curves similar to that shown in Figure 3A for experiments conducted at 296.3 K, a temperature well below the T_m for this mixture. These curves show pronounced deviations from the monoexponential behavior prescribed by eq 1 with $n = 1$ (dashed line). At the same time, fitting the attenuation curves by eq 1 with $n = 2$ produces satisfactory results (solid lines). This biexponential behavior indicates the existence of two ensembles of lipids with different diffusion coefficients. The smaller diffusion coefficient can be assigned to the l_o phase and the larger diffusion coefficient to the l_d phase. For any particular phase, the diffusivities of all lipid species present in that phase in multicomponent bilayers can be expected to be essentially the same or similar on the basis of the results of previous experimental studies.[25,26] This expectation is also confirmed by the data in Figure 3A showing that the diffusion behavior is the same for all lipids contributing to the measured choline signal (i.e., DOPC and DPPC).

Figure 3B−D shows qualitatively similar attenuation curves measured at 301.6, 300.7, and 298.9 K, respectively. As in Figure 3E, there is deviation from a single-exponential fit of the initial slope (dashed lines) indicating that a two-exponential fit using eq 1 with $n = 2$ (solid lines) provides a more appropriate description of the measured data. As the temperature approaches the T_m for this mixture, the extent of deviation from the single-exponential behavior becomes smaller (compare solid and dashed lines). This change could be a consequence of a change of diffusion coefficients, phase fractions, or a combination of the two. There is also a noticeable change in diffusion behavior with increasing effective diffusion time. Table 1 reports the best fit results for the curves in Figure 3, i.e., diffusivities and the corresponding fractions in the l_o and l_d phases. The error of data in the table has contributions from a number of sources including uncertainties associated with the calibration of gradient strength, sample preparation, the reproducibility of the measured PFG NMR attenuation curves, and the fitting of data using eq 1. For most measurements, the total error did not exceed ±10%. In some cases, the reported uncertainty was larger than ±10% due to a larger error associated with fitting the data by eq 1.

Figure 4 gives T_1 NMR relaxation curves measured for the line of the CH_3 choline group. The measurements were performed by the stimulated echo sequence for the same temperature range as that used in diffusion measurements. A series of one-dimensional PFG NMR STE experiments were carried out at each temperature using a gradient amplitude which was sufficiently small to ensure that there was no attenuation of the lipid signal due to diffusion but sufficiently large to suppress water signal. The delay (τ_2) between the second and third $\pi/2$ radiofrequency pulses in the sequence was varied over a range that corresponds to the range of t_{eff} values used in the PFG NMR STE diffusion measurements. During τ_2, the signal amplitude is reduced due to T_1 NMR relaxation by a factor of $\exp(-\tau_2/T_1)$. The normalized amplitude of the choline line was plotted against τ_2 along with curves which were obtained by fitting each set of data with either a biexponential or triexponential curve. The T_1 NMR relaxation curves show nonmonoexponential behavior at all temperatures including the highest temperature corresponding to the compositionally homogeneous bilayers (Figure 4). For highly resolved spectra of lipid bilayers in which lines of different proton types (i.e., choline, methylene, etc.) do not overlap, monoexponential T_1 plots are expected for each type of proton.[55,56] Each type of proton is capable of having unique relaxation behavior. Under our experimental conditions, the lines of the choline and methylene groups, which are expected to have different T_1 values, show a significant overlap (Figure 2). Hence, the nonmonoexponential behavior of the relaxation data at the highest temperature in Figure 4 can be attributed to the existence of such overlap. With decreasing temperatures, the line width of both CH_3 choline and CH_2 groups become broader leading to a more pronounced overlap.[57] The deviation from monoexponential behavior is therefore expected to become larger as temperature is decreased from 307.8 to 296.3 K. This expectation is in agreement with the data in Figure 4. In addition to the existence of signal overlap discussed above, the nonmonoexponential behavior of the T_1 plots at low

TABLE 1: Results from Fitting of the PFG NMR Attenuation Curves in Figure 3 by Equation 1[a]

t_{eff} (ms)	p_o	$D_o \times 10^{12}$ (m^2/s)	p_d	$D_d \times 10^{12}$ (m^2/s)
$T = 307.8$ K				
8.24			1	4.7 ± 0.5
14.24			1	4.7 ± 0.5
29.24			1	4.7 ± 0.5
59.24			1	4.6 ± 0.5
179.24			1	4.5 ± 0.4
$T = 301.6$ K				
8.24	0.24 ± 0.07	1.6 ± 0.2	0.76 ± 0.08	3.5 ± 0.3
14.24	0.19 ± 0.08	1.6 ± 0.2	0.81 ± 0.08	3.3 ± 0.3
29.24	0.14 ± 0.03	1.4 ± 0.1	0.87 ± 0.09	3.2 ± 0.3
59.24	0.11 ± 0.04	1.3 ± 0.3	0.89 ± 0.09	3.1 ± 0.3
179.24	0.02 ± 0.02	1.0 ± 0.4	0.97 ± 0.10	2.9 ± 0.3
$T = 300.7$ K				
8.24	0.69 ± 0.11	1.8 ± 0.2	0.31 ± 0.11	4.3 ± 0.8
14.24	0.62 ± 0.12	1.8 ± 0.2	0.38 ± 0.12	4.2 ± 0.8
29.24	0.52 ± 0.18	1.6 ± 0.2	0.48 ± 0.18	3.8 ± 0.7
59.24	0.41 ± 0.14	1.5 ± 0.2	0.59 ± 0.14	3.3 ± 0.5
179.24	0.21 ± 0.15	1.2 ± 0.5	0.79 ± 0.15	2.8 ± 0.3
239.24	0.17 ± 0.12	1.1 ± 0.4	0.83 ± 0.12	2.8 ± 0.3
$T = 298.9$ K				
8.24	0.73 ± 0.07	1.7 ± 0.2	0.27 ± 0.03	4.1 ± 0.4
14.24	0.61 ± 0.08	1.6 ± 0.2	0.39 ± 0.08	3.6 ± 0.6
59.24	0.49 ± 0.05	1.5 ± 0.2	0.49 ± 0.05	3.4 ± 0.3
179.24	0.18 ± 0.08	1.1 ± 0.2	0.82 ± 0.08	2.6 ± 0.3
239.24	0.15 ± 0.09	1.1 ± 0.2	0.85 ± 0.09	2.7 ± 0.3
$T = 296.3$ K				
14.24	0.70 ± 0.07	1.2 ± 0.1	0.30 ± 0.03	4.0 ± 0.7
29.24	0.63 ± 0.06	1.1 ± 0.1	0.37 ± 0.04	3.7 ± 0.4
59.24	0.57 ± 0.06	1.1 ± 0.1	0.43 ± 0.06	3.1 ± 0.3
119.24	0.53 ± 0.05	1.1 ± 0.1	0.47 ± 0.05	3.3 ± 0.3
179.24	0.44 ± 0.09	1.0 ± 0.1	0.56 ± 0.09	2.8 ± 0.3
239.24	0.42 ± 0.04	1.0 ± 0.1	0.58 ± 0.06	3.1 ± 0.3

[a] Given in the table are fractions and diffusivities of lipid ensembles for 307.8, 301.6, 300.7, 298.9, and 296.3 K, respectively.

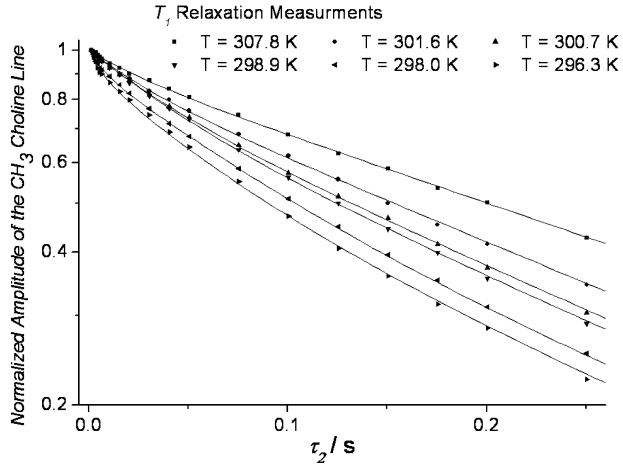

Figure 4. T_1 NMR relaxation curves obtained using the PFG NMR STE sequence with $g < 1$ T/m for a range of relevant temperatures. τ_2 denotes the delay between the second and third $\pi/2$ pulses of the sequence. The delay between the first and second $\pi/2$ pulse of the PFG NMR STE sequence was kept constant at 3.65 ms.

temperatures can be related to the inhomogeneous nature of the lipid bilayers exhibiting the existence of l_o and l_d phases. Clearly, the T_1 NMR times for CH_3 choline group can be different in different types of phases. The later can contribute to the observed deviations of the T_1 plots at low temperatures from the monoexponential behavior (see discussion below).

Discussion

One very significant characteristic of the data in Figure 3 is the manner in which diffusion behavior changes with effective diffusion time at temperatures below T_m (see Figure 3B−E). Effective diffusion times are directly related to the root-mean-square displacements of lipids according to the Einstein relation $\langle r^2(t)\rangle^{1/2} = (4Dt_{eff})^{1/2}$ for two-dimensional diffusion. Hence, the observed changes in the diffusion behavior can be directly attributed to the changes in the lipid displacements. If the l_o domains are much larger than the lipid displacements during the experimental observation time (t_{eff}) or do not exist at all, the PFG NMR attenuation curves for different t_{eff} values are expected to coincide with each other and give the same values of diffusivity within experimental error (see Figure 3A). In the case that the size of domains is comparable to the lipid displacements, diffusion behavior is expected to be dependent on the effective diffusion time.[58]

Figure 5 illustrates diffusion behavior at small (14.24 ms) and large (179.24 ms) values of t_{eff} for each temperature (below T_m) reported in Figure 3. In each case, the fraction of molecules attributed to the diffusion inside l_o domains decreases with an increase in t_{eff} which indicates an existence of exchange between l_o and l_d phases. The data in Figure 3 indicate that at the larger t_{eff}, most lipids diffuse either in the liquid-disordered phase or diffuse a fraction of the diffusion time in the liquid-ordered domains and the remaining fraction of diffusion time in the liquid-disordered phase. The diffusivity value of lipids in the liquid-disordered phase is ~2−3 times larger than that for the liquid-ordered phase (Table 1). For this reason, lipids that spend even a small fraction of the observation time in the liquid-disordered phase will be attributed to the liquid-disordered phase fraction because their overall effective diffusivity will be closer to that of the l_d rather than the l_o phase. The experimental observation that with increasing t_{eff} the decrease in the fraction of lipids attributed to the l_o phase is larger at $T = 301.6$ K than at lower temperatures (Figure 5A) indicates that the extent of exchange between the two phases is greater at this temperature.

It is important to note that, in addition to the lipid exchange between different types of domains, the observed dependence of the diffusion behavior on diffusion time (Figure 5) can be caused by an influence of the characteristic longitudinal NMR relaxation times (T_1) on the measured PFG NMR signal. Such influence can arise if the T_1 times are sufficiently short and different for the proton signal of the choline groups of lipids located in different phases. In this case, the contribution to the measured stimulated echo signal from lipids with smaller T_1 values would decrease with increasing diffusion time (note that $\tau_2 \approx t_{eff}$) relative to that corresponding to larger T_1 values. From the results in Figure 4, it can be concluded that for the same t_{eff}, the influence of T_1 NMR relaxation on the measured PFG NMR signal becomes larger with decreasing temperature. This is in agreement with the results of studies showing an increase in T_1 NMR relaxation rates of lipids in the same or similar types of lipid bilayers as the temperature decreases.[38,55,57] In addition, the difference between the values of T_1 in different phases can become more pronounced at smaller temperatures. The later is related to the expectation that many properties of the l_o and l_d phases, including NMR relaxation times, become more similar as the temperature is increased to approach the T_m. In agreement with this expectation, the deviations of the T_1 NMR relaxation curves in Figure 4 from the monoexponential behavior become slightly less pronounced with increasing temperature. The discussion above suggests that the influence of T_1 on the t_{eff} dependence of the fractions of lipids with different diffusivities has to be smaller at the temperatures near the transition temperature than at the temperatures much lower than the transition temperature. At the same time, the results in Table 1 and Figure 5 show that the t_{eff} dependence of the fractions of lipids with different diffusivities is much stronger at larger temperatures than at smaller temperatures. Hence, we can conclude that the possible disturbing influence of T_1 NMR relaxation cannot be of large significance for the observed t_{eff} dependencies of the diffusion behavior at temperatures near the transition temperature. As a result, our experimental data at these temperature(s) can be used to obtain quantitative information on the exchange of lipids between different types of domains and on the domain properties. In particular, we have attempted to estimate the permeability of the domain boundaries for diffusing lipids as well as sizes of l_o domains.

Figure 6 shows the results of fitting experimental data for $T = 300.7$ K with the corresponding results of the dynamic Monte Carlo simulations outlined above. Such a fitting procedure was recently introduced by one of the authors of this paper and his colleagues to determine surface permeability of nanoporous particles.[53] Figure 6A plots the ratio of the effective diffusivity of lipid molecules residing in l_o domains (D_o) to the diffusivity for the limiting case of small times when the diffusion is not influenced by the domain boundaries, $D_{o,t\to 0}$, as a function of diffusion time. The experimental value for $D_{o,t\to 0}$ was obtained from a linear extrapolation of D_o vs $\sqrt{t}$ (not shown here). Such type of extrapolation is frequently used to determine diffusivity in the limiting case of small diffusion times.[53,59] The simulated curves were obtained for the values of the permeability of domain boundary, α, corresponding to a range between the limiting case when the domain boundary provides no transport barriers for lipid molecules ($\alpha = 1.0 \times 10^{-3}$ m/s in Figure 6), and a value of α which is almost 2 orders of magnitude smaller ($\alpha = 2.0 \times 10^{-5}$ m/s in Figure 6). Figure 6A indicates that there is only an insignificant difference between the simulation

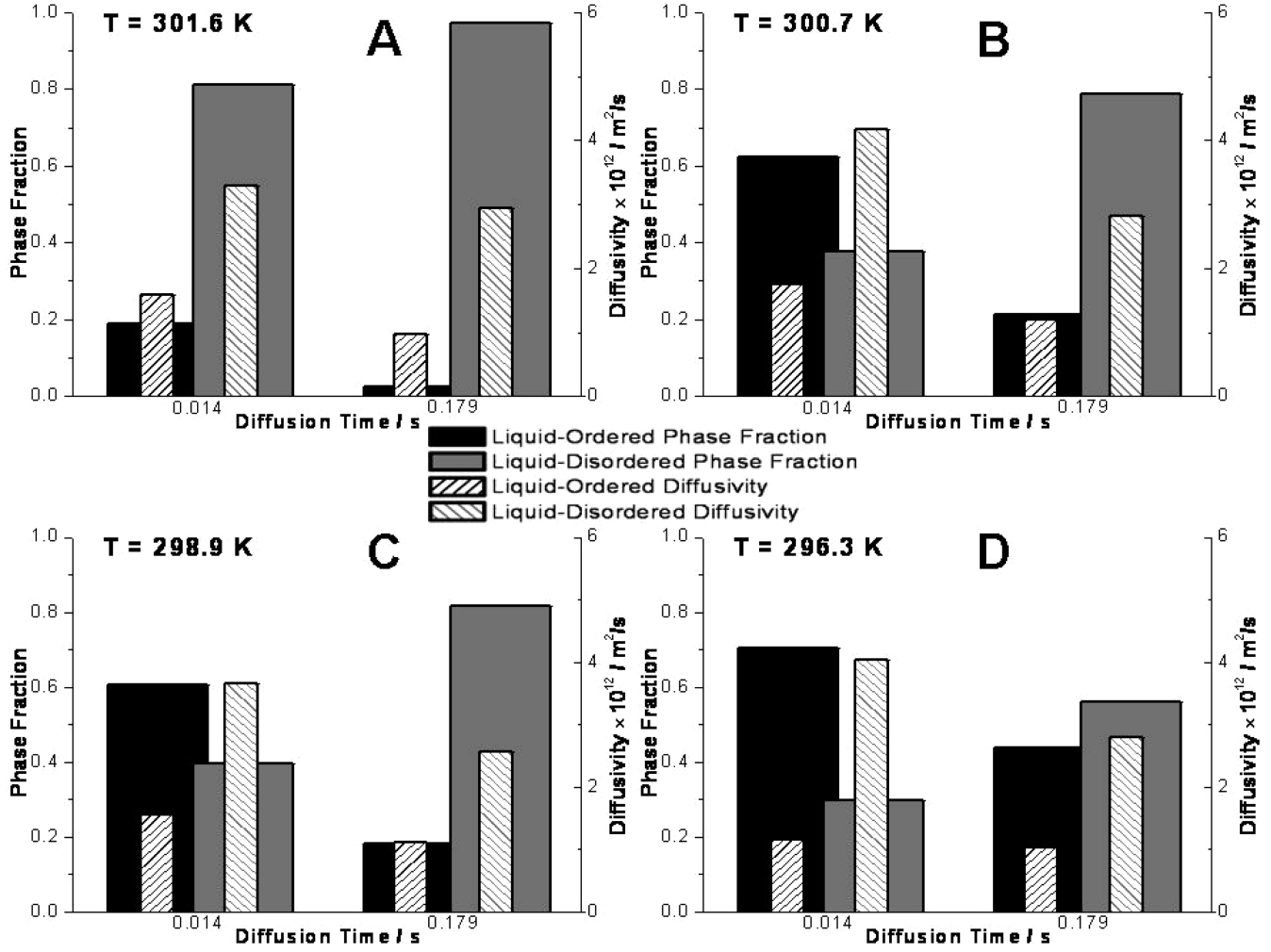

Figure 5. Comparison of diffusion behavior at different effective diffusion times for experiments conducted at 301.6 K (A), 300.7 K (B), 298.9 K (C), and 296.3 K (D). The amplitudes of the solid columns show the phase fractions (left vertical axis) of the l_o (black) and l_d (gray) phases while the amplitudes of the striped columns correspond to the diffusivities (right vertical axis) of the phases of solid columns on which they are superimposed.

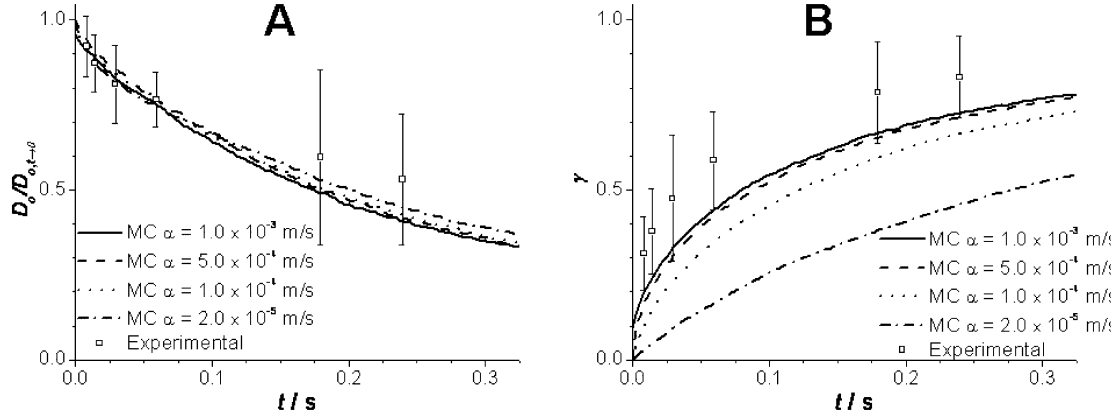

Figure 6. Examples of fitting experimental data (points) by the results of MC simulations (lines) for the following two dependencies: (A) time dependence of the ratio of the effective diffusivity of molecules in liquid-ordered domains to the corresponding unrestricted diffusivity in these domains (i.e., the diffusivity for the limiting case of small times) and (B) time dependence of the normalized fraction of molecules (γ) that started their trajectory inside the domains but ended their trajectory outside of domains. Experimental data was obtained at 300.7 K. The results of dynamic Monte Carlo (MC) simulations are shown for different permeabilities of the domain boundaries (α).

results for different barrier permeabilities used. These differences are especially small for the values of the ratio $D_o/D_{o,t\to 0}$ close to 1. Fitting the initial experimental data points (i.e., those at small times when α does not affect D_o) to the simulated curves in Figure 6A was used to determine the correlation between the experimental diffusion time and the diffusion time used in the simulation. The corresponding correlation between the length scales in the experiment and simulation was obtained by comparing the absolute values of diffusivities at a fixed time. Figure 6B shows a plot of the relative number of molecules, γ,

TABLE 2: Domain Properties at Temperatures Near T_m

	300.7 K	301.6 K
α, m/s	$\geq 5.0 \times 10^{-4}$	$\geq 9.2 \times 10^{-4}$
R_{l_o}, nm	930 ± 290	730 ± 310

which at initial time ($t = 0$) have started their trajectories inside l_o domains and were outside these domains by the time shown on the horizontal axis of the figure. Such dependencies are often referred to as tracer exchange curves. Since the relationship between the diffusion time in the experiment and simulation was already determined in Figure 6A, there are no "free" parameters that can be used to adjust the correspondence between the experimental and simulation data in Figure 6B. In contrast to the data in Figure 6A, there is a significant difference between the simulation data for different values of α in Figure 6B. It is seen in Figure 6B that within the experimental uncertainty, the experimental data agrees with the simulation results obtained for $\alpha \geq 5.0 \times 10^{-4}$ m/s. Hence, we estimate that the permeability of the l_o domain boundary to be greater than 5.0×10^{-4} m/s at 300.7 K. Using the relationship between the length scales in the experiment and simulations as well as the domain size used in the simulations, we estimate the domain radius (R_{l_o}) to be 930 ± 290 nm at 300.7 K. These estimates for α and R_{l_o} were obtained assuming that all domains are circular and there is no distribution over domain sizes as well as over permeabilities of the domain boundaries and intradomain diffusivities. Clearly, using an assumption that at least some of such distributions exist would allow obtaining an even better agreement between the experimental and simulation data in Figure 6B. The size of the square domains used in simulations was used to determine the radius of the corresponding circular domains by equating the surface area-to-perimeter ratios for both domain shapes. Similar treatment of the experimental data recorded at 301.6 K resulted in $\alpha \geq 9.2 \times 10^{-4}$ m/s and $R_{l_o} = 730 \pm 310$ nm (Table 2).

A PFG NMR diffusion study of supported multibilayer stacks with the same composition as that used in the present work was previously reported.[60] In contrast to this previous study, much larger gradients were used in the present work. This opened the possibility of the analysis of the permeability of the domain boundaries reported above. Comparison between the absolute values of the lipid diffusivities reported here and in ref 55 shows a reasonably good agreement between the measured diffusivities. In particular, the difference between the lipid diffusivities at 309 K when only an l_d phase exists does not exceed 20%. The corresponding differences between the diffusivities reported here and in ref 55 for l_d and l_o phases at lower temperatures in all cases do not exceed a factor of around 2.

Conclusion

PFG NMR at high field and high gradient strength was used to directly monitor the exchange of lipids between l_o and l_d domains formed in ternary lipid bilayers. This experimental option provides the possibility to monitor diffusion over length scales which are comparable to the size of l_o domains in membranes. Exchange was observed to occur over the time scales of the experimental diffusion times and was found to become more pronounced as the bilayer temperature was increased toward the miscibility transition temperature. The latter can be explained by an increase in diffusivity and some decrease in the characteristic domain sizes with an increase in temperature. Comparison of the experimental data and the corresponding results of dynamic Monte Carlo simulations allowed estimating domain boundary permeability and domain size at temperatures near the transition temperature. The observed size of domains is still quite large in comparison to the minimum displacement that can be observed with our experimental setup. It is then quite possible and would be very interesting to use this technique to study the exchange of lipids between domains in systems that form even smaller, biologically relevant l_o domains.

Acknowledgment. NMR data were obtained at the Advanced Magnetic Resonance Imaging and Spectroscopy (AMRIS) facility in the McKnight Brain Institute of the University of Florida. We thank Dr. D. Plant for numerous discussions.

References and Notes

(1) Brown, D. A.; London, E. *Annu. Rev. Cell Dev. Biol.* **1998**, *14*, 111.
(2) Singer, S. J.; Nicolson, G. L. *Science* **1972**, *175*, 720.
(3) Simons, K.; Ikonen, E. *Nature* **1997**, *387*, 569.
(4) Simons, K.; Toomre, D. *Nat. Rev. Mol. Cell. Biol.* **2000**, *1*, 31.
(5) Patra, S. K. *Biochim. Biophys. Acta (BBA)—Rev. Cancer* **2008**, *1785*, 182.
(6) Fantini, J.; Garmy, N.; Mahfoud, R.; Yahi, N. *Expert Rev. Molec. Medicine* **2002**, *20*, 1.
(7) Ahmed, S. N.; Brown, D. A.; London, E. *Biochemistry* **1997**, *36*, 10944.
(8) Dietrich, C.; Bagatolli, L. A.; Volvyk, Z. N.; Thompson, N. L.; Levi, M.; Jacobson, K.; Gratton, E. *Biophys. J.* **2001**, *80*, 1417.
(9) Sengupta, P.; Holowka, D.; Baird, B. *Biophys. J.* **2007**, *92*, 3564.
(10) Silvius, J.; Nabi, I. R. *Molec. Membrane Biol.* **2006**, *23*, 5.
(11) de Almeida, R. F. M.; Loura, L. S.; Fedorov, A.; Prieto, M. *J. Mol. Biol.* **2005**, *346*, 1109.
(12) Kahya, N.; Schwille, P. *Molec. Membrane Biol.* **2006**, *23*, 29.
(13) Crane, J. M. Fluorescence Microscopy to Study Domains in Supported Lipid Bilayers. In *Methods in Membrane Lipids*; Dopico, A., Ed.; Humana Press: Totowa, NJ, 2007; Vol. 400; p 481.
(14) Korlach, J.; Schwille, P.; Webb, W. W.; Feigenson, G. *Proc. Natl. Acad. Sci. U.S.A.* **1999**, *96*, 8461.
(15) Bacia, K.; Scherfeld, D.; Kahya, N.; Schwille, P. *Biophys. J.* **2004**, *87*, 1034.
(16) Shaw, J. E.; Epand, R. F.; Epand, R. M.; Li, Z.; Bittman, R.; Yip, C. M. *Biophys. J.* **2006**, *90*, 2170.
(17) Samiee, K. T.; Moran-Mirabal, J. M.; Cheung, Y. K.; Craighead, H. G. *Biophys. J.* **2006**, *90*, 3288.
(18) Edel, J. B.; Wu, M.; Baird, B.; Craighead, H. G. *Biochim. Biophys. Acta (BBA)—Biomembranes* **2005**, *1668*, 158.
(19) Yuan, C.; Furlong, J.; Burgos, P.; Johnston, L. J. *Biophys. J.* **2002**, *82*, 2526.
(20) Tokumasu, F.; Jin, A. J.; Feigenson, G. W.; Dvorak, J. A. *Biophys. J.* **2003**, *84*, 2609.
(21) Johnston, L. J. *Langmuir* **2007**, *23*, 5886.
(22) Forstner, M. B.; Martin, D. S.; Navar, A. M.; Kas, J. A. *Langmuir* **2003**, *19*, 4876.
(23) Lindblom, G. r.; Orädd, G. *J. Dispersion Sci. Technol.* **2007**, *28*, 55.
(24) Polozov, I. V.; Gawrisch, K. *Biophys. J.* **2006**, *90*, 2051.
(25) Orädd, G.; Westerman, P. W.; Lindblom, G. *Biophys. J.* **2005**, *89*, 315.
(26) Scheidt, H. A.; Huster, D.; Gawrisch, K. *Biophys. J.* **2005**, *89*, 2504.
(27) Lindblom, G.; Orädd, G. *Prog. Nucl. Magn. Reson. Spectrosc.* **1994**, 483.
(28) Filippov, A.; Orädd, G.; Lindblom, G. *Biophys. J.* **2004**, *86*, 891.
(29) Filippov, A.; Orädd, G.; Lindblom, G. *Biophys. J.* **2003**, *84*, 3079.
(30) Ulrich, K.; Sanders, M.; Grinberg, F.; Galvosas, P.; Vasenkov, S. *Langmuir* **2008**, *24*, 7365.
(31) Ulrich, K.; Sanders, M.; Vasenkov, S. *Magn. Reson. Imag.* **2007**, *25*, 493.
(32) Varma, R.; Mayor, S. *Nature* **1998**, *394*, 798.
(33) Mayor, S.; Rao, M. *Traffic* **2004**, *5*, 231.
(34) Pralle, A.; Keller, P.; Florin, E. L.; Simons, K.; Horber, J. K. H. *J. Cell Biol.* **2000**, *148*, 997.
(35) Veatch, S. L.; Polozov, I. V.; Gawrisch, K.; Keller, S. L. *Biophys. J.* **2004**, *86*, 2910.
(36) Holland, G. P.; McIntyre, S. K.; Alam, T. M. *Biophys. J.* **2006**, *90*, 4248.
(37) Silvius, J. R. *Biophys. J.* **2003**, *85*, 1034.

(38) Veatch, S. L.; Soubias, O.; Keller, S. L.; Gawrisch, K. *Proc. Natl. Acad. Sci. U.S.A.* **2007**, *104*, 17650.
(39) Radhakrishnan, A.; McConnell, H. *J. Chem. Phys.* **2007**, *126*, 185101.
(40) Nielsen, L. K.; Bjornholm, T.; Mouritsen, O. G. *Nature* **2000**, *404*, 352.
(41) Gomez, J.; Sagues, F.; Reigada, R. *Phys. Rev. E* **2008**, *77*, 021907.
(42) Pandit, S. A.; Jakobsson, E.; Scott, H. L. *Biophys. J.* **2004**, *87*, 3312.
(43) Garbès Putzel, G.; Schick, M. *Biophys. J.* **2008**, *94*, 869.
(44) Mitra, P.; Halperin, B. *J. Magn. Reson. A* **1995**, *113*, 94.
(45) Malmborg, C.; Topgaard, D.; Soderman, O. *J. Magn. Reson.* **2004**, *169*, 85.
(46) Lindblom, G.; Orädd, G.; Filippov, A. *Chem. Phys. Lipids* **2006**, *141*, 179.
(47) Filippov, A.; Orädd, G.; Lindblom, G. *Biophys. J.* **2006**, *90*, 2086.
(48) Cotts, R. M.; Hoch, M. J. R.; Sun, T.; Markert, J. T. *J. Magn. Reson.* **1989**, *83*, 252.
(49) Orädd, G.; Lindblom, G. *Magn. Reson. Chem.* **2004**, *42*, 123.
(50) Krutyeva, M.; Kärger, J. *Langmuir* **2008**, *24*, 10474.
(51) Krutyeva, M.; Vasenkov, S.; Kärger, J. *Magn. Reson. Imag.* **2007**, *25*, 567.
(52) Krutyeva, M.; Vasenkov, S.; Yang, X.; Caro, J.; Kärger, J. *Microporous Mesoporous Mater.* **2007**, *104*, 89.
(53) Krutyeva, M.; Yang, X.; Vasenkov, S.; Kärger, J. *J. Magn. Reson.* **2007**, *185*, 300.
(54) Gibbs, S. J.; Johnson, C. S. *J. Magn. Reson.* **1991**, *93*, 395.
(55) Deese, A. J.; Dratz, E. A.; Hymel, L.; Fleischer, S. *Biophys. J.* **1982**, *37*, 207.
(56) Kroon, P. A.; Kainosho, M.; Chan, S. I. *Biochim. Biophys. Acta* **1976**, *433*, 282.
(57) Kroon, P. A.; Kainosho, M.; Chan, S. I. *Biochim. Biophys. Acta (BBA)—Biomembranes* **1976**, *433*, 282.
(58) Lindblom, G.; Orädd, G. *Biochim. Biophys. Acta (BBA)—Biomembranes* **2009**, *1788*, 234.
(59) Latour, L. L.; Mitra, P. P.; Kleinberg, R. L.; Sotak, C. H. *J. Magn. Reson., Ser. A* **1993**, *101*, 342.
(60) Orädd, G.; Westerman, P. W.; Lindblom, G. *Biophys. J.* **2005**, *89*, 315.

JP9057093

Influence of Water on Diffusion in Imidazolium-Based Ionic Liquids: A Pulsed Field Gradient NMR study

Amrish Menjoge,[†] JaNeille Dixon,[‡] Joan F. Brennecke,[‡] Edward J. Maginn,[‡] and Sergey Vasenkov*,[†]

Department of Chemical Engineering, University of Florida, Gainesville, Florida 32611, and Department of Chemical and Biomolecular Engineering, University of Notre Dame, Notre Dame, Indiana 46556

Received: January 30, 2009; Revised Manuscript Received: March 19, 2009

In this work, we applied a novel pulsed field gradient (PFG) NMR option, which combines advantages of high-field (17.6 T) NMR and high magnetic field gradients (up to 30 T/m), to study diffusion of anions, cations and water in two 1-ethyl-3-methylimidazolium-based ionic liquids. Application of high field allows for an easy recording of an NMR signal from small amounts of water added to the ionic liquids. Using high gradients is advantageous because under conditions of such gradients any susceptibility-induced inhomogeneities in the local magnetic field are expected to be negligibly small in comparison with the applied gradients. PFG NMR studies have been performed in a broad range of temperatures and for different diffusion times. The effect of water addition on the diffusion behavior of the anions and cations is discussed in the context of the presence of polar and nonpolar domains in the ionic liquids. A partial screening of the electrostatic interaction between the cations and anions in the polar domains by water is believed to be responsible for the following changes in the diffusion behavior, which were observed experimentally: (i) increase in the ion diffusivities with increasing water concentration, and (ii) decrease in the difference between the diffusion coefficient of the cation and that of the anion as water concentration increases.

Introduction

Molten salts, which are liquid at temperatures around room temperature, are referred to as room temperature ionic liquids (RTILs). Many RTILs exhibit a number of interesting properties such as an excellent solubility for polar and nonpolar compounds, negligible vapor pressure, large liquidus range (viz. range of temperature between normal melting and boiling point/decomposition temperature), high ionic conductivity, and good thermal stability. All these properties make RTILs a very attractive type of media for chemical reactions and separations.[1] In addition, RTILs can be used as heat transfer/storage fluids, lubricants, etc.[1−4]

RTILs are usually hygroscopic. As a result, they can absorb significant amounts of water.[1,5−7] Even those RTILs that are sometimes considered to be hydrophobic show an ability to absorb water from the surrounding gas phase.[8,9] It has been demonstrated that various properties of ionic liquids such as solubility, polarity, viscosity, and conductivity depend on the water content.[1,7,8] An addition of water can also change chemical reactions of solutes in RTILs. For example, the influence of water was observed for oxygenation of toluene in the presence of palladium in the 1-*n*-butyl-3-methylimidazolium tetrafluoroborate ([bmim][BF_4]) ionic liquid. For this reaction an addition of water can lead to a change of the main product from benzaldehyde to benzoic acid.[10]

Nanostructural organization of aqueous solutions of ionic liquids and its changes with increasing water concentration have been a focus of many recent studies.[7,11−25] In particular, investigations using a number of methods, which include IR spectroscopy and density functional calculations, revealed the formation of hydrogen bonds between water and anions in imidazolium-based ionic liquids.[6,21,24,25] These studies showed that at low water concentrations water exists in a nonself-aggregated state. In this case, water molecules form complexes mostly with anions rather than with other water molecules. The data discussed above are in a qualitative agreement with the results of recent molecular dynamics (MD) simulations, which indicate that water molecules in RTILs tend to be isolated from each other at small water concentrations.[11,22,23] In contrast, a water percolation cluster can be formed at high water concentrations corresponding to molar fractions of water ≥75%.[11]

The results of MD simulations reported in refs 11, 12, and 22 show that for sufficiently small water concentrations diffusion coefficients of ions in aqueous solutions of RTILs increase continuously with increasing water content. This observation is supported by the data provided by electrochemical measurements of ion transport rates in aqueous solutions of ionic liquids.[26] Here we report the results of direct studies of an influence of water content on diffusion of ionic species and water in the RTILs containing the same cation 1-ethyl-3-methylimidazolium ([emim]$^+$) and two different anions, ethylsulfate ([$EtSO_4$]$^-$) and triflate ([TfO]$^-$). The diffusion studies were carried out by proton-pulsed field gradient (PFG) NMR technique. PFG NMR was previously applied to investigate diffusion in RTILs (see, for example, refs 27−32). However, until now a systematic study of an influence of water on the collective process of ion diffusion in imidazolium-based RTILs in a large temperature range has not been reported. This gap is filled by the present work. A comparison is also made between experimentally measured self-diffusivities and those obtained from previous MD simulations for [emim][$EtSO_4$].[23]

* To whom correspondence should be addressed. Phone: +1 352 392 0315. Fax: +1 352 392 0315. E-mail: svasenkov@che.ufl.edu.
[†] University of Florida.
[‡] University of Notre Dame.

10.1021/jp900902n CCC: $40.75
Published on Web 04/10/2009

Experimental Section

Materials. RTILs containing the same type of cation (1-ethyl-3-methylimidazolium ($[emim]^+$)) and two different types of anions (ethylsulfate ($[EtSO_4]^-$) and triflate ($[TfO]^-$)) were used. Mixtures of the RTILs and water were prepared by adding weighted amounts of water into the water-free RTILs. The water concentration in the studied samples of the RTILs was varied in the range between 0 and 15% w/w.

The IL [emim][$EtSO_4$] and [emim][TfO] were purchased from Solvent Innovation (both >99% purity). The samples were dried by rotary evaporation and heating under high vacuum (<67 Pa) for two days. The water mass fraction of the final products was less than 500 ppm, as measured by Karl Fischer titration with a Metrohm 831 KF Coulometer.

Sample Preparation. The pure RTILs or aqueous solutions of RTILs were introduced into the standard 5 mm NMR tubes. The mixtures were prepared in glass vials and mixed well before taking the appropriate size sample out for each NMR tube. In all cases the sample height in a vertically oriented tube was ≤15 mm. This height was sufficiently small to ensure the absence of disturbing convection effects under our measurement conditions at elevated temperatures. After loading with RTIL samples, the NMR tubes were flame sealed to avoid changes in the water content.

We have shown[33] that [emim][$EtSO_4$] can degrade in the presence of water to form [emim][HSO_4]. However, the degradation is a slow process leading to a decomposition of only 28% or less of [emim][$EtSO_4$] over the period of 1.5 or more years. The [emim][$EtSO_4$]/water samples used in this study were made with fresh [emim][$EtSO_4$] and tested within 2 weeks after preparation. Therefore, we believe the results are for primarily [emim][$EtSO_4$] mixtures.

Pulsed Field Gradient (PFG) NMR Studies. ^{1}H PFG NMR diffusion studies were carried out using a wide bore Bruker Biospin NMR spectrometer operating at a proton resonance frequency of 750 MHz. Magnetic field gradients were generated using a diff60 diffusion probe (Bruker Biospin) and a Great60 gradient amplifier (Bruker Biospin). Diffusion measurements of ions and water were performed using the standard PFG NMR stimulated echo pulse sequence[34,35] in a broad range of temperatures between 288 and 354 K. In most cases it was sufficient to use gradients with the maximum amplitude of around 10 T/m.

Diffusion data were obtained from dependencies of the intensity of the PFG NMR signal (A) on the amplitude of the magnetic field gradients (g). The signal intensity was determined by integrating the area under selected line(s) of the frequency-domain NMR spectra recorded by the PFG NMR stimulated echo pulse sequence. Different lines in such spectra can correspond to different species. Hence, diffusion data for a chosen type of species in a sample can be obtained by selecting an appropriate line in the spectrum for data processing. For the NMR lines exhibiting no significant overlap with the lines of other types of ions or molecules in a sample the diffusivity (D) was determined from the measured attenuation of the PFG NMR signal ($\Psi \equiv A(g)/A(g=0)$) corresponding to this line using[34,35]

$$\Psi = \exp(-(\gamma\delta g)^2 D t_{\mathrm{eff}}) \qquad (1)$$

where γ is the gyromagnetic ratio, δ denotes the effective duration for rectangular gradient pulses, g is the amplitude of the magnetic gradients, t_{eff} is the effective diffusion time ($t_{\mathrm{eff}} = \Delta - (\delta/3)$), and Δ is the separation between the gradient pulses. When a selected NMR line has a contribution from two or three different types of molecules and/or ions having different diffusivities, the attenuation curves were described as a sum of two or three weighted exponential terms of the type shown in eq 1

$$\Psi = \sum_{i=1}^{n=2\mathrm{or}3} A_i \exp(-(\gamma\delta g)^2 D_i t_{\mathrm{eff}}) \qquad (2)$$

where A_i and D_i represent the fraction and diffusivity of species i, respectively, and n is the number of different species contributing to the NMR line.

The signal attenuation was measured under the conditions when only the value of g was varied and all other parameters in the PFG NMR stimulated echo sequence remained constant. The value of δ was in all cases much smaller than Δ, thus $t_{\mathrm{eff}} \approx \Delta$. The effective diffusion time was changed by changing the value of Δ. For each temperature the measurements were performed for at least two effective diffusion times equal to 24.78 and 49.78 ms.

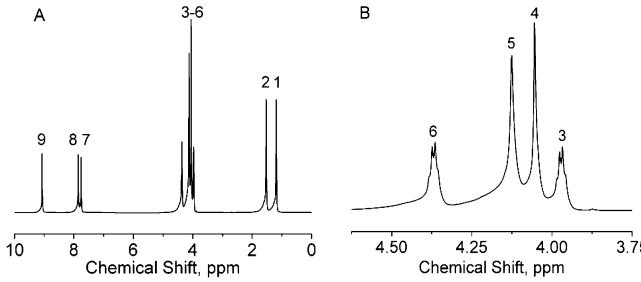

Figure 1. ^{1}H NMR spectrum of [emim][$EtSO_4$] containing 10% (w/w) water. (A) For chemical shifts in the range between 0 and 10 ppm to show all lines. (B) For chemical shifts in the range between 3.75 and 4.625 ppm to show lines 3−6.

Results and Discussion

Figure 1 shows an example of ^{1}H NMR spectra of [emim][$EtSO_4$] containing water. The spectrum in Figure 1 was recorded using the free induction decay (FID) sequence.[34,35] The NMR lines labeled 2, 4, 6, 7, 8, and 9 are assigned to the $[emim]^+$ cation,[36]while lines 1 and 3 are assigned to the $[EtSO_4]^-$ anion. The line 5 is attributed to water.[37] The lines 2 and 6 originate from the protons of the ethyl chain of $[emim]^+$, while the line 4 belongs to the protons of the methyl group attached to the imidazolium ring of the cation. The lines 7, 8, and 9 can be assigned to the protons of the imidazolium ring. The lines 1 and 3 belong to the protons of the ethyl side chain of $[EtSO_4]^-$. The chemical shift of the water line (5) was observed to shift downfield with increasing water concentration. Such changes in the chemical shift can be attributed to a decrease in the extent of hydrogen bonding between water and anions with increasing water concentration.[37] The corresponding proton NMR spectra recorded for [emim] [TfO] (see Supporting Information) were similar to those presented in Figure 1 with the exception of the $[EtSO_4]^-$ lines. As expected, the latter lines were absent in the [emim][TfO] spectra. There was no contributions from $[TfO]^-$ in these spectra because $[TfO]^-$ are proton-free ions.

In all studied samples the NMR line of water showed some overlap with the lines corresponding to either anion, cation, or both. An extent of the overlap was different for different water concentrations due to strong dependence of the chemical shift of the water line on the water concentration.

Figure 2 shows examples of the PFG NMR attenuation curves measured for [emim][$EtSO_4$] containing water. It is seen in Figure 2 that the attenuation curves for $[emim]^+$ and $[EtSO_4]^-$ are monoexponential in agreement with eq 1. This is an expected

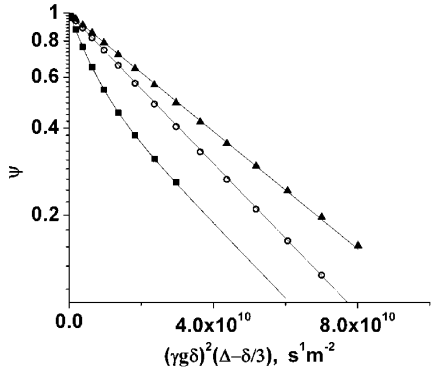

Figure 2. Proton PFG NMR attenuation curves measured for the sample of [emim][$EtSO_4$] containing 7% (w/w) water for $t_{eff} = 49.33$ ms at $T = 288$ K. The data are shown for the $[emim]^+$ line at 1.5 ppm (○), the $[EtSO_4]^-$ line at 1.2 ppm (▲), and the water line at 4.2 ppm (□). The latter line has a contribution from the $[emim]^+$ lines centered at 4.38 and 4.07 ppm. Solid curves show the best fit results using eq 1 for the cation and anion and using eq 2 with $n = 2$ for water. Equation 2 was used due to the existence of an overlap between the water and $[emim]^+$ lines.

behavior because the cation and anion lines at the chemical shifts of 1.5 ppm (no. 2) and 1.2 ppm (no. 1), which were used to measure these attenuation curves, represent the pure lines with no noticeable contribution from other types of molecules or ions. It was verified that for different pure lines originating from the same type of species the measured proton PFG NMR attenuation curves remained the same within the experimental uncertainty.

Figure 2 also shows that the attenuation curve for water deviates significantly from the monoexponential behavior predicted by eq 1. This deviation is assigned to the existence of an overlap of the water line at 4.2 ppm with the neighboring $[emim]^+$ lines centered at 4.38 and 4.07 ppm. The analysis of the changes of the line shape with increasing gradient strength confirmed this assignment. The PFG NMR attenuation curve corresponding to this line was fitted by eq 2 with $n = 2$ and D_2 equal to the diffusivity of $[emim]^+$ (Figure 2). This allowed determining the water diffusivity, that is, D_1 in eq 2. The same type of fitting procedure was employed to determine water diffusivities in all other cases.

Tables 1 and 2 present proton PFG NMR diffusion data for the [emim][TfO] and [emim] [$EtSO_4$] samples, respectively. The diffusivities were obtained for at least two effective diffusion times equal to 24.8 and 49.8 ms and for two values of the time interval between the first and the second (π)/(2) pulses of the PFG NMR stimulated echo sequence (τ)[34,35] equal to 1.5 and 3.0 ms. For each temperature and water concentration, the measured ion diffusivities at different values of t_{eff} and τ remained the same within an uncertainty less than ±10%. This uncertainty was used as an experimental uncertainty for ion diffusivities. The experimental uncertainty for water diffusivity was in some cases higher due to the existence of an overlap between the NMR line of water and those of ions. It is important to note that all diffusion data were obtained by proton PFG NMR, which allowed simultaneous and high-precision monitoring of diffusivities of all proton-containing species in the samples. No data are shown for $[TfO]^-$ because these ions are proton-free. The diffusion data is presented in the tables only for the temperatures smaller than the following two temperatures: (i) the temperature corresponding to an onset of condensation of water in an upper part of the NMR tubes with the RTIL samples and (ii) the temperature corresponding to the appearance of a noticeable dependence of the measured effective diffusivity on diffusion time due to convection effects. Both condensation and convection effects prevented reliable PFG NMR measurements at temperatures larger than those given in Tables 1 and 2. These effects occurred due to the existence of a temperature gradient in sealed NMR tubes with the RTIL samples under our measurement conditions at elevated temperatures.

Previous MD simulations[23] on [emim][$EtSO_4$] found self-diffusivities for the cation and anion to be a factor of 2−3 lower than the PFG NMR values. This discrepancy is typical of that observed for other ionic liquid systems and is likely due to deficiencies in the force fields used to model interactions between the ions. Interestingly, however, the MD simulations are consistent with the PFG NMR findings that the cation has a slightly higher self-diffusivity than the anion.

It was observed that in the temperature range used in this study the temperature dependencies of the measured diffusivities can be described by the Arrhenius law

$$D = D_0 \exp(-E/RT) \quad (3)$$

where E is the activation energy for diffusion, R is the gas constant, and D_0 denotes the pre-exponential factor. Figure 3 shows some examples of the measured temperature dependencies.

Figure 4 shows dependencies of the activation energy for diffusion on water concentration in [emim][TfO] and [emim]-[$EtSO_4$]. It is seen that the change of the water concentration from zero to around 0.7 water molecules per anion−cation pair leads to a noticeable drop in the activation energy. A further increase in the water concentration leaves the activation energy essentially unchanged within the experimental uncertainty. A clear correlation was observed between the concentration dependencies of the activation energy (Figure 4) and the corresponding concentration dependencies for the ion diffusivities. Examples of the latter dependencies are shown in Figure 5 for a selected temperature of 298 K. Qualitatively similar results were obtained for all other temperatures used in this study.

It is seen in Figure 5 that an increase in the water concentration from 0 to ca. 0.7 water molecules per anion−cation pair results in a significant increase in the ion diffusivities at 298 K. This correlates with a decrease in the activation energy for diffusion observed for the same change in the water concentration (Figure 4). An addition of more water to the RTIL samples after this initial change of the water concentration leads to a less pronounced increase in the ion diffusivities. The values of the reciprocal viscosity[38] show the same general trend as the ion diffusivities (Figure 5), that is, they increase with increasing water concentration. In the presentation of Figure 5, the extent of this increase becomes smaller with increasing water concentration.

It is interesting to note that in the water-free sample of [emim][$EtSO_4$] the diffusivity of a more bulky cation is approximately a factor of 2 larger than that of a less bulky anion (Figure 5B). The data in Figure 5 show that this anomalous difference in the diffusivities decreases significantly with increasing water concentration. The exact same behavior was observed in the MD simulations (see Supporting Information).[23]

For both types of ionic liquids, the diffusivity of water in the ionic liquid was found to increase gradually with increasing water concentration (Figure 5). The diffusivity values of water in the RTIL samples were much larger than those of the ions but at the same time much smaller than the corresponding diffusivity of pure water (2.3×10^{-9} m^2 s^{-1} at 298 K).[39]

Recent experimental studies and computer simulations have shown that RTILs exhibit the existence of polar and nonpolar regions.[7,12,40−42] The imidazolium-based RTILs containing imi-

TABLE 1: Diffusivities of $[emim]^+$ and Water Recorded by Proton PFG NMR in the Samples of [emim][TfO] with Different Water Concentrations and at Different Temperatures[a]

	Diffusivity × 10^{10}(m^2 s^{-1})					
	288 K	298 K	309 K	321 K	335 K	354 K
			0% (w/w) water			
$[emim]^+$	0.28 ± 0.01	0.40 ± 0.02	0.66 ± 0.03	1.00 ± 0.05	1.70 ± 0.17	2.90 ± 0.30
water	n/a	n/a	n/a	n/a	n/a	n/a
			5% (w/w) water			
$[emim]^+$	0.66 ± 0.03	0.90 ± 0.05	1.19 ± 0.06	1.50 ± 0.15	2.00 ± 0.32	
water	3.60 ± 0.36	4.70 ± 0.48	5.80 ± 0.59	8.00 ± 1.19		
			7% (w/w) water			
$[emim]^+$	0.80 ± 0.04	1.10 ± 0.06	1.40 ± 0.07	1.58 ± 0.16	2.00 ± 0.34	
water	3.70 ± 0.37	4.70 ± 0.48	6.60 ± 0.66	8.0 ± 1.2	11.0 ± 2.2	
			10% (w/w) water			
$[emim]^+$	1.09 ± 0.05	1.50 ± 0.08	1.80 ± 0.19			
water	4.40 ± 0.44	5.70 ± 0.57	8.0 ± 1.2			
			12% (w/w) water			
$[emim]^+$	1.16 ± 0.12	1.56 ± 0.16				
water	3.97 ± 0.6	6.00 ± 0.89				
			14% (w/w) water			
$[emim]^+$	1.33 ± 0.13	1.91 ± 0.19				
water	4.00 ± 0.68	6.00 ± 0.93				

[a] The experimental uncertainty reflects deviations between the diffusivities measured at the same water concentration and temperature but for different diffusion times and different delays between the first and the second $\pi/2$ pulses of the PFG NMR stimulated echo sequence. It also reflects deviations between the corresponding data obtained using different NMR lines of the same type of species under the same measurement conditions.

TABLE 2: Diffusivities of $[emim]^+$, $[EtSO_4]^-$, and Water Recorded by Proton PFG NMR in the Samples of [emim][$EtSO_4$] with Different Water Concentrations and at Different Temperatures[a]

	Diffusivity × 10^{11}(m^2 s^{-1})					
	288 K	298 K	309 K	321 K	335 K	354 K
			0% (w/w) water			
$[emim]^+$		1.19 ± 0.06	2.20 ± 0.11	3.80 ± 0.19	6.90 ± 0.69	12.00 ± 1.2
$[EtSO_4]^-$		0.7 ± 0.04	1.31 ± 0.07	2.39 ± 0.12	4.55 ± 0.46	9.00 ± 0.86
water		n/a	n/a	n/a	n/a	n/a
			5% (w/w) water			
$[emim]^+$	2.80 ± 0.14	4.37 ± 0.22	6.40 ± 0.32	9.42 ± 0.47	13.00 ± 0.13	
$[EtSO_4]^-$	2.10 ± 0.11	3.29 ± 0.16	4.86 ± 0.24	7.00 ± 0.35	10 ± 0.99	
water	17.9 ± 0.9	22.5 ± 1.1	30.0 ± 3.0	41.00 ± 4.1	59.0 ± 8.8	
			7% (w/w) water			
$[emim]^+$	3.60 ± 0.18	5.70 ± 0.28	8.0 ± 0.41	12.0 ± 0.61		
$[EtSO_4]^-$	2.84 ± 0.14	4.35 ± 0.22	6.59 ± 0.33	9.75 ± 0.49		
water	19.00 ± 0.96	24.00 ± 1.2	31.00 ± 3.1	41.0 ± 4.1		
			10% (w/w) water			
$[emim]^+$	5.00 ± 0.25	7.60 ± 0.38	11.00 ± 0.57	15.0 ± 1.5		
$[EtSO_4]^-$	3.93 ± 0.20	6.07 ± 0.30	9.00 ± 0.45	12.0 ± 1.2		
water	18.0 ± 0.92	27.0 ± 1.4	40.0 ± 4.0	54.0 ± 8.2		
			12% (w/w) water			
$[emim]^+$	5.80 ± 0.29	7.91 ± 0.40	10.5 ± 1.0			
$[EtSO_4]^-$	4.80 ± 0.24	6.55 ± 0.33	9.00 ± 0.85			
water	23.0 ± 1.1	31.4 ± 1.6	38.0 ± 5.7			
			14% (w/w) water			
$[emim]^+$	6.56 ± 0.33	9.79 ± 0.49	14.0 ± 1.4			
$[EtSO_4]^-$	5.80 ± 0.29	8.00 ± 0.41	12.0 ± 1.2			
water	25.0 ± 1.3	38.0 ± 1.9	50.0 ± 7.6			

[a] The experimental uncertainty reflects deviations between the diffusivities measured at the same water concentration and temperature but for different diffusion times and different delays between the first and the second $\pi/2$ pulses of the PFG NMR stimulated echo sequence. It also reflects deviations between the corresponding data obtained using different NMR lines of the same type of species under the same measurement conditions.

dazolium cations with small ($\leq C_3$) alkyl side chains are known to form many discontinuous nonpolar regions in a sea of a continuous three-dimensional network of polar domains.[12] The results of previous experimental and computational investigations suggest that an addition of small amounts of water into such ionic liquids leads to a formation of complexes between water and ions.[11,12,21−24,43,44] For sufficiently small water concentrations such complexes can be described as symmetric 1:2 H-bonded complexes, anion···HOH···anion. Under these conditions water molecules tend to be isolated from each

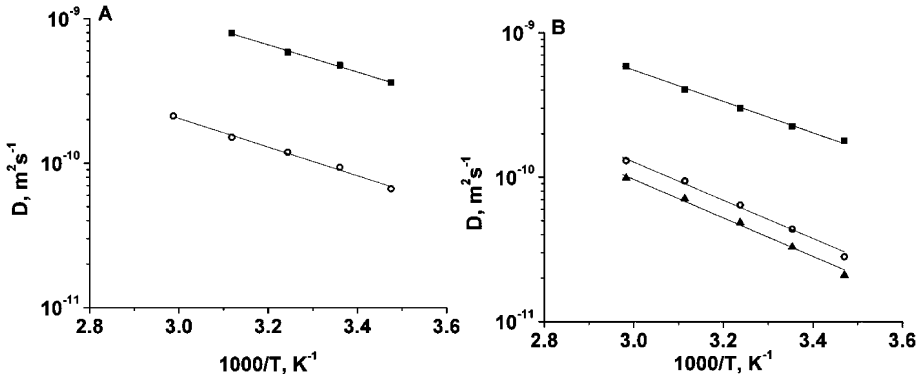

Figure 3. Temperature dependencies of the measured diffusivity of $[emim]^+$ (○), $[EtSO_4]^-$ (▲), and water (□) (A) for the aqueous solution of [emim][TfO] with 5% (w/w) water and (B) for the aqueous solution of [emim] $[EtSO_4]$ with 5% (w/w) water. Solid lines show the best fit results using eq 3.

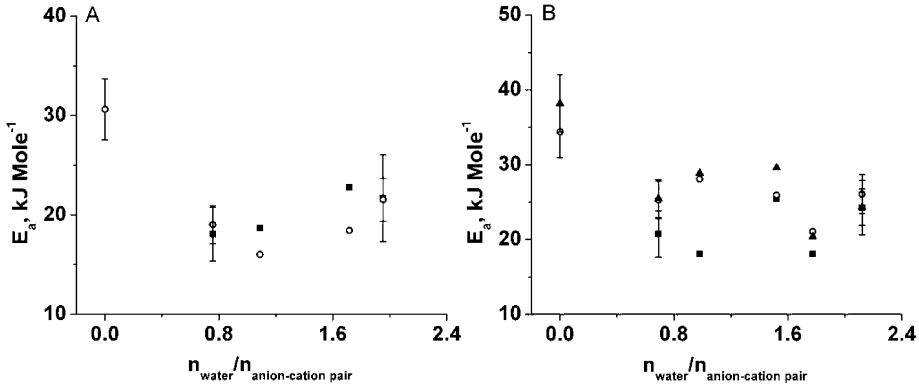

Figure 4. Dependencies of the activation energy for diffusion on water concentration, which is presented as a number of water molecules per anion−cation pair ($n_{water}/n_{anion-cation\ pair}$), for $[emim]^+$ (○),$[EtSO_4]^-$ (▲), and water (□). (A) For [emim][TfO]. (B) For [emim][$EtSO_4$].

other.[11,22,23] However, at large water concentrations (≥75% molar) a percolating network of water can be formed.[11]

The results shown in Figures 4 and 5 may be explained based on the nanostructural organization of RTILs discussed above. When a small amount of water molecules is introduced into the water-free RTILs, these molecules are incorporated into the polar domains,[12] which are formed by the charged head groups of the cation and anion. The water molecules are expected to form anion···HOH···anion type complexes through hydrogen bonding. This behavior was observed in previous computational and experimental studies.[22−24,44] As a result of the formation of such complexes, the electrostatic interactions between the cations and anions become partially screened by water. Such screening of the electrostatic interactions could be the reason for the observed decrease in the activation energies for ion diffusion and a corresponding increase in the ion diffusivities (Figures 4 and 5). The smallest nonzero water concentration used in this study (around 0.7 water molecules per anion−cation pair) was sufficiently large to ensure that all anions in the samples can form H-bonds with water because each water molecule is capable of forming such bonds with two anions. Hence, an increase in the water concentration beyond this initial level would not lead to any increase in the number of the anions which directly interact with water molecules. The absence of a major qualitative change in the local environment of the anions due to such additional increases in the water concentration explains why the corresponding changes of the ion diffusivities and of the activation energies for diffusion of ions become smaller after the first change in the water concentration from 0 to around 0.7 water molecules per anion−cation pair. (Figures 4 and 5). A further increase in the water concentration after this initial change can result in the formation of secondary hydrogen bonds

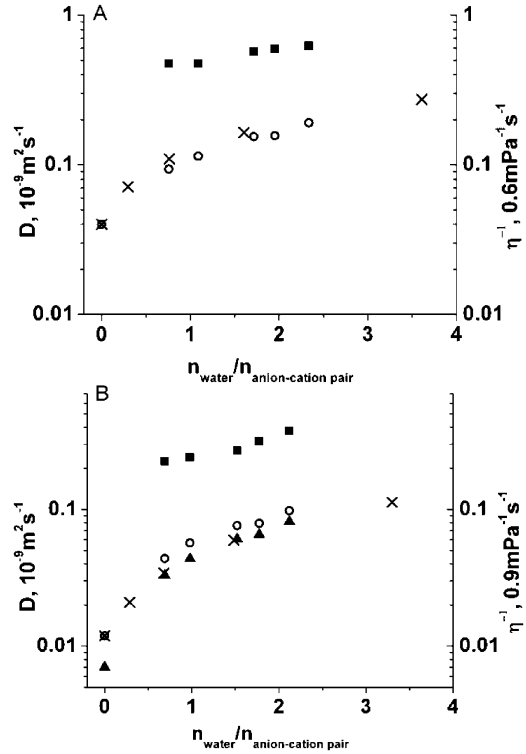

Figure 5. Diffusivities of $[emim]^+$ (○),$[EtSO_4]^-$ (▲), and water (□) measured by proton PFG NMR as a function of the number of water molecules per anion−cation pair at 298 K (A) for [emim][TfO] and (B) for [emim][$EtSO_4$]. Also shown for comparison are the values of the reciprocal viscosity (×) for these ionic liquids at the same temperature as reported by Rodriguez H. and Brennecke J.[38]

of water with the existing anion···HOH···anion complexes and/or lead to the formation of small clusters of water molecules.[11,12] It is important to note that even at the largest water concentration used (around 2.3 water molecules per anion−cation pair) the water concentration remains too small for the formation of the percolation water cluster. As a result, the water diffusivity in the studied samples was in all cases much smaller than the diffusivity of pure water.

The unusual diffusion behavior observed in the experiments and MD simulations (i.e., the bulkier cation has a larger self-diffusivity than the anion) has been observed for different types of RTILs[22,23,27,32,45] and has been explained as being due to anisotropic displacement of the ions; displacement along the ring plane and perpendicular to a vector between the two ring nitrogen atoms is favored over other displacement directions.[46] The electrostatic interactions that lead to ordering of the liquid on nanometer length scales may result in this motion being favored. It is not universally observed, however. PFG NMR and MD simulations of pyridinium-based ionic liquids with bis(trifluoromethanesulfonyl)amide anions have shown that the larger cations can have smaller self-diffusivities than the anions.[28]

An addition of water was observed to reduce significantly the magnitude of the anomalous difference between the diffusivities of the cations and anions (Figure 5). This can be attributed to a partial screening of the electrostatic interaction between the cations and anions by water molecules. As a result of such screening the domain structure is expected to become more fluid and the cooperative character of the ion diffusion less pronounced.

For diffusion of hard spheres in a continuum solvent the relationship between viscosity and diffusivity obeys the Stokes−Einstein relation

$$D = \frac{kT}{C\pi\eta r_s} \tag{4}$$

where k is the Boltzmann constant, C is a constant and r_s is the effective hydrodynamic (Stokes) radius. The existence of strong interactions between cations and anions is expected to limit the use of this expression for RTILs.[27,47−49] The results of a recent computational study[25] show that the nonvalidity of eq 4 can be related to dynamical heterogeneities in RTILs. Nevertheless, a good correlation between the reciprocal viscosity and the diffusivity of the largest species in the studied RTIL samples, that is, the $[emim]^+$ cations, was observed in all cases (Figure 5). A somewhat poorer correlation between the reciprocal viscosity and the diffusivity of the $[EtSO_4]^-$ anions measured for different water concentrations (Figure 5B) can be attributed to the fact that an increase in the water concentration transforms the anions from the smallest (at zero water concentration) to the second largest (at nonzero water concentration) species in the studied RTIL samples.

Conclusion

This paper reports the results of PFG NMR diffusion study of imidazolium-based RTILs with and without water. It was observed that the presence of water in the RTILs at the concentration slightly larger than one water molecule per two anion−cation pairs leads to a significant change in the values of diffusivities and activation energies for diffusion of ions in comparison with those in the corresponding water-free samples. A further increase of the water concentration resulted in less pronounced changes in the parameters characterizing ion diffusion. This behavior can be understood by noticing that the initial water concentration of around one water molecule per two anion−cation pairs is already sufficiently high to ensure the formation of hydrogen bonds between each anion and water. Hence, an increase of the water concentration beyond this initial level would not lead to an increase in the number of anions directly interacting with water. In the water-free ionic liquid $[emim][EtSO_4]$, the diffusivity of the bulkier $[emim]^+$ cation was found to be larger than that of the less bulky $[EtSO_4]^-$ anion. This anomalous relationship between the size and diffusivity of diffusing species can be attributed to the existence of well-defined local structures in RTILs resulting in a cooperative character of ion diffusion and even in an appearance of diffusion anisotropy for the cation diffusion. With increasing water concentration these structures could become progressively less defined leading to a change toward normal relationship between the size and diffusivity of diffusing species.

Acknowledgment. NMR data were obtained at the Advanced Magnetic Resonance Imaging and Spectroscopy (AMRIS) facility in the McKnight Brain Institute of the University of Florida. We thank Dr. Dan Plant, AMRIS for his help with NMR measurements. The financial support from DOE (Grant DE-FG02-05CH11294-001) is gratefully acknowledged.

Supporting Information Available: This material is available free of charge via the Internet at http://pubs.acs.org.

References and Notes

(1) Welton, T. *Chem. Rev.* **1999**, *99*, 2071.
(2) Brennecke, J. F.; Maginn, E. J. *AIChE J.* **2001**, *47*, 2384.
(3) *Novel Ionic Liquid Thermal Storage for Solar Thermal Electric Power Systems*, Proceedings of the International Solar Energy Conference: a part of Forum 2001, Solar Energy, The Power to Choose; April 21−25, 2001, Washington, D.C. Wu, B.; Reddy, R. G.; Rogers, R. D. Eds.; American Society of Mechanical Engineers, New York, N. Y., 2001.
(4) Chiappe, C.; Pieraccini, D. *J. Phys. Org. Chem.* **2005**, *18*, 275.
(5) Aki, S. N. V. K.; Brennecke, J. F.; Samanta, A. *Chem. Commun.* **2001**, 413.
(6) Tran, C. D.; Silvia, H.; Lacerda, D. P.; Oliveira, D. *Appl. Spectrosc.* **2003**, *57*, 152.
(7) Chiappe, C. *Monatsh. Chem.* **2007**, *138*, 1035.
(8) Seddon, K. R.; Stark, A.; Torres, M.-J. *Pure Appl. Chem.* **2000**, *72*, 2275.
(9) Huddleston, J. G.; Visser, A. E.; Reichert, W. M.; Willauer, H. D.; Broker, G. A.; Rogers, R. D. *Green Chem.* **2001**, *3*, 156.
(10) Seddon, K. R.; Stark, A. *Green Chem.* **2002**, *4*, 119.
(11) Hanke, C. G.; Lynden-Bell, R. M. *J. Phys. Chem. B* **2003**, *107*, 10873.
(12) Jiang, W.; Wang, Y.; Voth, G. A. *J. Phys. Chem. B* **2007**, *111*, 4812.
(13) Jungnickel, C.; Luczak, J.; Ranke, J.; Fernandez, J. F.; Mueller, A.; Thoeming, J. *Colloids Surf., A* **2008**, *316*, 278.
(14) Dong, B.; Zhang, J.; Zheng, L.; Wang, S.; Li, X.; Inoue, T. *J. Colloid Interface Sci.* **2008**, *319*, 338.
(15) Inoue, T.; Ebina, H.; Dong, B.; Zheng, L. *J. Colloid Interface Sci.* **2007**, *314*, 236.
(16) Mukherjee, P.; Crank, J. A.; Halder, M.; Armstrong, D. W.; Petrich, J. W. *J. Phys. Chem. A* **2006**, *110*, 10725.
(17) Miskolczy, Z.; Sebok-Nagy, K.; Biczok, L.; Goektuerk, S. *Chem. Phys. Lett.* **2004**, *400*, 296.
(18) Anderson, J. L.; Pino, V.; Hagberg, E. C.; Sheares, V. V.; Armstrong, D. W. *Chem. Commun.* **2003**, 2444.
(19) Goodchild, I.; Collier, L.; Millar, S. L.; Prokes, I.; Lord, J. C.; Butts, C. P.; Bowers, J.; Webster, J. R.; Heenan, R. K. *J. Colloid Interface Sci.* **2007**, *307*, 455.
(20) Bowers, J.; Butts, C. P.; Martin, P. J.; Vergara-Gutierrez, M. C. *Langmuir* **2004**, *20*, 2191.
(21) Cammarata, L.; Kazarian, S. G.; Salter, P. A.; Welton, T. *Phys. Chem. Chem. Phys.* **2001**, *3*, 5192.
(22) Kelkar, M. S.; Maginn, E. J. *J. Phys. Chem. B* **2007**, *111*, 4867.
(23) Kelkar, M. S.; Shi, W.; Maginn, E. J. *J. Ind. Eng. Chem. Res.* **2008**, *47*, 9115.
(24) Wulf, A.; Köddermann, T.; Wertz, C.; Heintz, A.; Ludwig, R. *Z. Phys. Chem.* **2006**, *220*, 1361.

(25) Köddermann, T.; Ludwig, R.; Paschek, D. *ChemPhysChem* **2008**, *9*, 1851.

(26) Schroder, U.; Wadhawan, J. D.; Compton, R. G.; Marken, F.; Suarez, P. A. Z.; Consorti, C. S.; Souza, R. F.; Dupont, J. *New J. Chem.* **2000**, *24*, 1009.

(27) Tokuda, H.; Hayamizu, K.; Ishii, K.; Susan, A. B. H.; Watanabe, M. *J. Phys. Chem. B* **2004**, *108*, 16593.

(28) Cadena, C.; Zhao, Q.; Snurr, R. Q.; Maginn, E. J. *J. Phys. Chem. B* **2006**, *110*, 2821.

(29) Judeinstein, P.; Iojoiu, C.; Sanchez, J.-Y.; Ancian, B. *J. Phys. Chem. B* **2008**, *112*, 3680.

(30) Annat, G.; MacFarlane, D. R.; Forsyth, M. *J. Phys. Chem. B* **2007**, *111*, 9018.

(31) Tokuda, H.; Tsuzuki, S.; Susan, M. A. B. H.; Hayamizu, K.; Watanabe, M. *J. Phys. Chem. B* **2006**, *110*, 19593.

(32) Noda, A.; Hayamizu, K.; Watanabe, M. *J. Phys. Chem. B* **2001**, *105*, 4603.

(33) Ficke, L. E.; Rodriǵuez, H. C.; Brennecke, J. F. *J. Chem. Eng. Data* **2008**, *53*, 2112.

(34) Callaghan, P. T. *Principles of NMR Microscopy*; Clarendon Press: Oxford, 1991.

(35) Kärger, J.; Ruthven, D. M. *Diffusion in Zeolites and Other Microporous Solids*; Wiley & Sons: New York, 1992.

(36) Heimer, N. E.; Sesto, R. E. D.; Carper, W. R. *Magn. Reson. Chem.* **2004**, *42*, 71.

(37) Singh, T.; Kumar, A. *J. Phys. Chem. B* **2007**, *111*, 7843.

(38) Rodriguez, H.; Brennecke, J. F. *J. Chem. Eng. Data* **2006**, *51*, 2145.

(39) Mills, R. *J. Phys. Chem.* **1973**, *77*, 685.

(40) Wang, Y.; Voth, G. A. *J. Am. Chem. Soc.* **2005**, *127*, 12192.

(41) Canongia Lopes, J. N. A.; Padua, A. A. H. *J. Phys. Chem. B* **2006**, *110*, 3330.

(42) Triolo, A.; Russina, O.; Bleif, H.-J.; Di Cola, E. *J. Phys. Chem. B* **2007**, *111*, 4641.

(43) Saha, S.; Hamaguchi, H. *J. Phys. Chem. B* **2006**, *110*, 2777.

(44) Köddermann, T.; Wertz, C.; Heintz, A.; Ludwig, R. *Angew. Chem., Int. Ed.* **2006**, *45*, 3697.

(45) Every, H. A.; Bishop, A. G.; MacFarlane, D. R.; Oradd, G.; Forsyth, M. *Phys. Chem. Chem. Phys.* **2004**, *6*, 1758.

(46) Urahata, S. M.; Ribeiro, M. C. C. *J. Chem. Phys.* **2005**, *122*, 024511.

(47) Tokuda, H.; Hayamizu, K.; Ishii, K.; Susan, M. A. B. H.; Watanabe, M. *J. Phys. Chem. B* **2005**, *109*, 6103.

(48) Tokuda, H.; Ishii, K.; Susan, M. A. B. H.; Tsuzuki, S.; Hayamizu, K.; Watanabe, M. *J. Phys. Chem. B* **2006**, *110*, 2833.

(49) Sediak, M. Structure and dynamics of polyelectrolite solutions by light scattering. In *Physical Chemistry of Polyelectrolytes*, V.99. Radeva, T., Ed.; CRC Press: Boca Raton, 2001; p 341.

JP900902N